EXTENDED REPORT

Reduced expression of autotaxin predicts survival in uveal melanoma

Arun D Singh, Karen Sisley, Yaomin Xu, Jianbo Li, Pieter Faber, Sarah J Plummer, Hardeep S Mudhar, Ian G Rennie, Patricia M Kessler, Graham Casey, Bryan G Williams

Br J Ophthalmol 2007;**91**:1385–1392. doi: 10.1136/bjo.2007.116947

See end of article for authors' affiliations

Correspondence to: Professor A D Singh, Director, Department of Ophthalmic Oncology, Cole Eye Institute, Cleveland Clinic Foundation, 9500 Euclid Avenue, Cleveland, OH 44195, USA; singha@ccf.org

Accepted 1 April 2007
Published Online First 2 May 2007

Aim: In an effort to identify patients with uveal melanoma at high risk of metastasis, the authors undertook correlation of gene expression profiles with histopathology data and tumour-related mortality.

Methods: The RNA was isolated from 27 samples of uveal melanoma from patients who had consented to undergo enucleation, and transcripts profiled using a cDNA array comprised of sequence-verified cDNA clones representing approximately 4000 genes implicated in cancer development. Two multivariate data mining techniques—hierarchical cluster analysis and multidimensional scaling—were used to investigate the grouping structure in the gene expression data. Cluster analysis was performed with a subset of 10 000 randomly selected genes and the cumulative contribution of all the genes in making the correct grouping was recorded.

Results: Hierarchical cluster analysis and multidimensional scaling revealed two distinct classes. When correlated with the data on metastasis, the two molecular classes corresponded very well to the survival data for the 27 patients. Thirty two discrete genes (corresponding to 44 probe sets) that correctly defined the molecular classes were selected. A single gene (ectonucleotide pyrophosphatase/phosphodiesterase 2; autotaxin) could classify the molecular types. The expression pattern was confirmed using real-time quantitative PCR.

Conclusions: Gene expression profiling identifies two distinct prognostic classes of uveal melanoma. Underexpression of autotaxin in class 2 uveal melanoma with a poor prognosis needs to be explored further.

About 5% of all melanomas arise from the ocular and adnexal structures and uveal melanoma is the most common primary intraocular malignant tumour with an incidence of approximately 4.3 cases per million per year in the USA.[1 2] Although, cutaneous and uveal melanocytes share a common embryologic origin, uveal melanoma and cutaneous melanoma have many differing clinical, epidemiological and prognostic features.[3 4]

The five-year survival rates following enucleation, brachytherapy and other methods of treatment of primary uveal melanoma range from 6%–53% depending upon the size of the tumour.[5–10] Despite achieving great accuracy in diagnosing uveal melanoma,[11] mortality from uveal melanoma in the USA has remained unchanged over a period of 25 years from 1973 to 1997.[12]

Recent studies have identified specific chromosomal changes of prognostic significance such as monosomy 3, alteration of 8q, and 6p[13–16] but the genetic mechanisms involved in the pathogenesis of uveal melanoma remain unknown. Microarray gene profiling of uveal melanoma tumour samples[17] and cell cultures[18] has revealed two subtypes of uveal melanoma. One previous study has suggested a correlation between molecular classes of uveal melanoma and survival.[19] To get a better insight into genes that are involved in uveal melanoma tumorigenesis and metastasis, we analysed gene expression profiles in 27 patients with uveal melanoma with known survival outcome.

MATERIALS AND METHODS

Tumour collection

The tumour specimens were collected from the eyes of patients undergoing enucleation. The tumour samples were snap frozen in liquid nitrogen at the point of collection, and subsequently transferred to −180°C for long-term storage.

Clinical data

Twenty seven patients with medium to large sized uveal melanoma were included in the study following approval by the institutional review board. The clinical details (age, sex), tumour features (location, largest basal diameter, height), histopathological features (per cent epithelioid component, presence or absence of matrix patterns), and outcome (follow-up duration, survival status (alive, dead due to metastasis, dead due to other causes)) were recorded for each patient. On the largest tumour face, a periodic acid-Schiff stain was carried out, without counterstain, to assess the tumour extracellular matrix patterns. Nine morphological patterns of extracellular matrix deposition have been defined for ciliary body or choroidal melanomas.[20 21] The presence of extracellular closed loops and networks (a network is defined as at least three back-to-back closed loops), is the feature strongly associated with death from metastatic disease.[20 21]

RNA isolation and target RNA preparation

RNA was isolated from uveal melanoma tumour samples using the RNAqueous kit (Ambion) as described by the manufacturer. Following isolation, the RNA was DNAse treated using the reagents from the DNA-free kit (Ambion, Foster City, USA), again as described by the manufacturer. The quality of the isolated RNA was verified using an Agilent 2100 Bioanalyzer (Agilent, Santa Clara, USA). Target RNA was generated in a T7 polymerase-based linear amplification reaction using a modified version of a published protocol.[22] Two micrograms of total RNA and 5 pmol of T7-(dT)24 primer [5′-GGCCAGTGAATTGTAATACGACTCACTATAGGGAGGCGG-(dT)24-3′] in a total volume of 5.5 µl was incubated at 70°C for 10 min and chilled on ice. For first-strand cDNA synthesis, the annealed RNA template was incubated for 1 h at 42°C in a 10 µl reaction mixture containing first-strand buffer (Invitrogen, Carlsbad,

Table 1 Clinical and pathologic profile of 27 patients with uveal melanoma

	Clinical			Tumour features				
No	Age (years)	Sex	Location	LBD (mm)	Height (mm)	E (%)	Networks	Outcome
202	45	Male	Choroid	16	11	0	Absent	Alive
205	73	Male	CBD + choroid	14	8	70	Present	Dead (Other)
209	64	Female	Choroid	15	7	30	Present	Dead (Mets)
212	45	Male	Choroid	17	1	30	Present	Dead (Mets)
213	71	Female	CBD + choroid	17	13	40	Absent	Dead (Mets)
218	42	Male	Choroid	13	6	30	Present	Dead (Mets)
222	36	Female	Choroid	12	7	5	Absent	Alive
232	67	Male	CBD + choroid	12	12	40	Present	Dead (Mets)
234	69	Male	CBD + choroid	19	12	30	Present	Dead (Mets)
235	71	Female	CBD + choroid	14	14	10	Present	Dead (Mets)
236	63	Male	CBD + choroid	21	9	10	Present	Dead (Mets)
237	49	Male	Choroid	22	8	0	Present	Dead (Mets)
239	43	Female	Choroid	16	8	10	Present	Dead (Mets)
240	35	Female	Choroid	17	8	0	Absent	Alive
242	83	Male	CBD + choroid	11	10	30	Present	Dead (Mets)
245	44	Male	Choroid	12	12	0	Absent	Alive
249	66	Male	Choroid	9	10	0	Absent	Alive
250	60	Female	Choroid	19	13	10	Absent	Dead (Mets)
253	50	Male	CBD + choroid	16	12	0	Absent	Alive
255	63	Female	CBD + choroid	17	8	1	Present	Dead (Mets)
256	80	Female	Choroid	10	5	1	Absent	Alive
263	70	Male	Choroid	13	8	10	Absent	Alive
266	61	Female	Choroid	16	9	0	Present	Alive
267	49	Female	Choroid	17	9	0	Absent	Alive
268	78	Female	Choroid	17	9	40	Present	Dead (Mets)
280	85	Male	Choroid	18	15	20	Absent	Dead (Mets)
289	88	Female	Choroid	19	10	40	Present	Dead (Mets)

LBD, largest basal diameter; E%, percent epithelioid component; Networks, presence or absence of aggressive matrix patterns; CBD, ciliary body; Mets, metastasis.

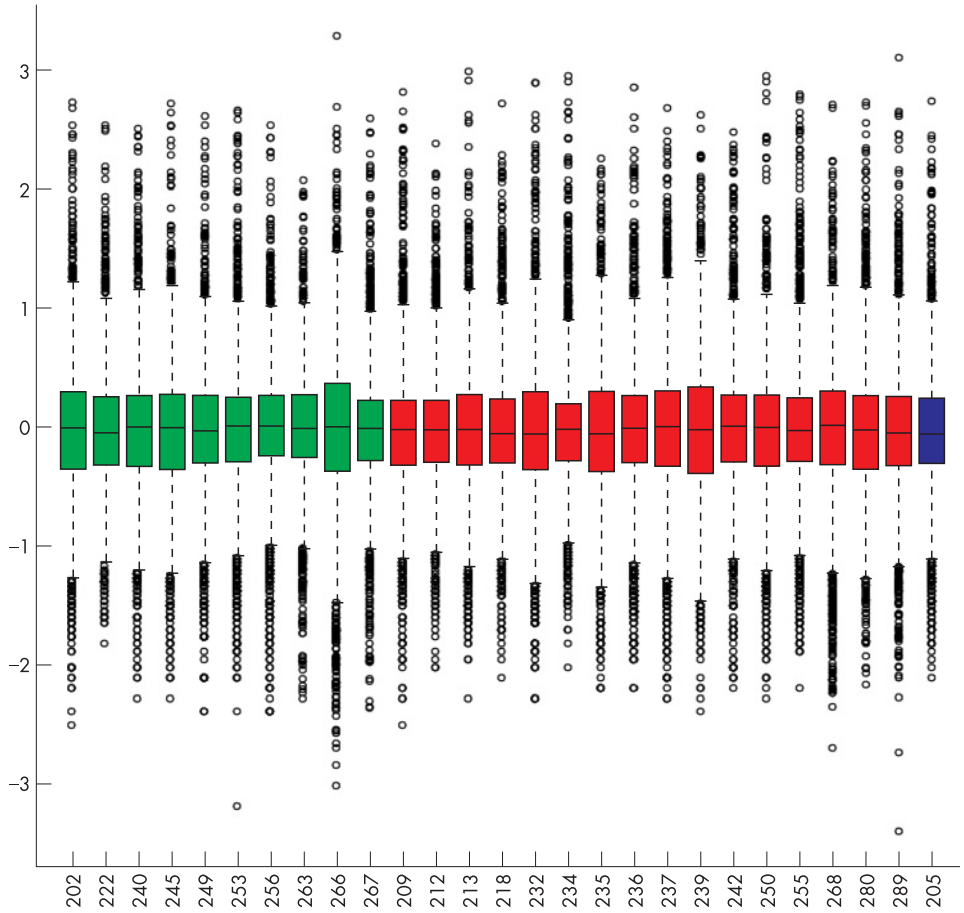

Figure 1 Box plot of the 27 tumour samples. The colour indicates the metastatic death status (green for alive, red for dead, and blue for death from other cause).

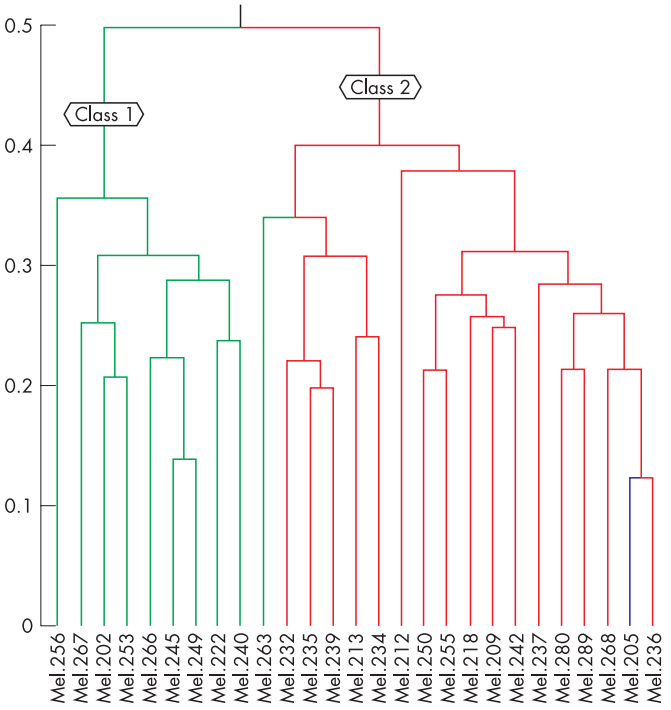

Figure 2 Dendrogram from the hierarchical cluster analysis using Pearson correlation as distance matrix. Two molecular classes were found, the one in the green box corresponds to class 1 that contains all the patients alive and the other one in the red box corresponds to class 2 with all people dead except for one alive.

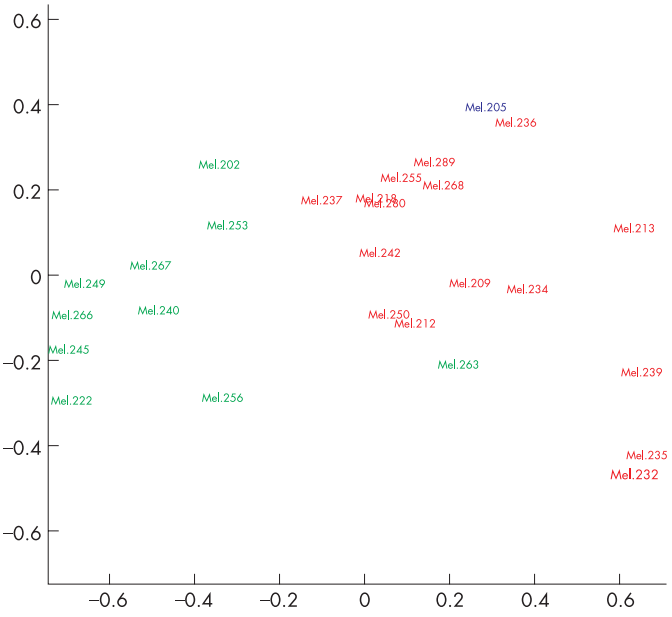

Figure 3 Plot of the multidimentional scaling with Pearson correlation as distance matrix. Two molecular classes, class 1 and class 2, are obvious and the colour indicates the metastatic death (green, alive; red, metastatic death; blue, one death of other cause).

CA, USA), 10 mM dithiothreitol, 1 unit of anti-RNase (Ambion) per µl, 500 µM deoxynucleoside triphosphates, and 2 units of Superscript II (Invitrogen) per µl. Second-strand synthesis was for 2 h at 16℃ in a total reaction volume of 50 µl containing first-strand reaction products, second-strand buffer (Invitrogen), 250 µM deoxynucleoside triphosphates, 0.06 unit of DNA ligase (Ambion) per µl, 0.26 unit of DNA polymerase I (New England Biolabs, Ipswich, USA) per µl, and 0.012 U of RNase H (Ambion) per µl followed by the addition of 3.3 units of T4 DNA polymerase (3 units per µl; New England Biolabs) and a further 15 min of incubation at 16℃. Second-strand reaction products were purified by phenol-chloroform-isoamyl alcohol extraction in Phaselock microcentrifuge tubes (Eppendorf, Westbury, NY, USA) according to the manufacturer's instructions and ethanol precipitated. In vitro transcription was performed by using the T7 megascript kit (Ambion) according to a modified protocol in which purified cDNA was combined with 1 µl (each) of 10× ATP, GTP, CTP, and UTP and 1 µl of T7 enzyme mix in a 10 µl reaction volume and incubated for 9 h at 37℃. Amplified RNA was purified by using the RNAeasy RNA purification kit (QIAGEN, Valencia, USA) according to the manufacturer's instructions.

cDNA microarray construction

The tumour cDNA array used in this study comprised a subset of sequence-verified cDNA clones from Research Genetics Inc (Carlsbad, USA), a 40 000-clone set representing approximately 4000 genes involved in tumorigenesis.[23–25] The 4000 cDNAs were selected based on their implication in metastasis and cancer development in general from the literature and from the Affymetrix cancer G110 array, the presence of AU-rich elements in their 3′- and/or 5′-untranslated region[25] as well as encoding proteins responsive to cytokines, containing a zinc-finger or being implicated in apoptosis. The complete list of spotted cDNAs on this tumour array can be downloaded from the site http://geacf.cwru.edu/geacf/geaaspotteddescriptions.shtml. DNA preparation and slide printing were as previously described, except for the use of 40% dimethyl sulfoxide in place of 1.5× SSC as the printing solution.[25]

RNA labelling

Cy3- or Cy5-labeled cDNA was prepared by indirect incorporation. Two micrograms of amplified RNA, 1 µl of dT12-18 primer (1 µg per µl; Invitrogen), 2.6 µl of random hexanucleotides (3 µg per µl; Invitrogen), and 1 µl of anti-RNase (Ambion) were combined in a reaction volume of 15.5 µl and incubated for 10 min at 70℃. Reverse transcription was for 2 h at 42℃ in

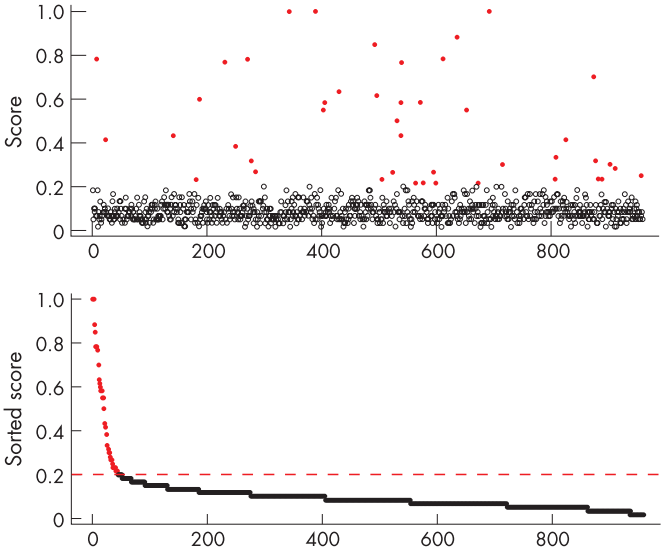

Figure 4 Top key genes selected from the selection algorithm. Gene weights was the average gene selection rate, and 20% was used as the cutoff to select the key genes that were correctly defined the molecular class 1 and class 2.

Table 2 Summary of the properties of the 32 key genes (44 probe sets)

Gene*	Score†	Mean ratio‡	p Value§	Common	Genbank	UniGene
20026	1	1.6	9.40E-03	Sarcoglycan, delta (35 kda dystrophin-associated glycoprotein)	AA234982	Hs.387207
20194	1	0.22	4.30E-07	Ectonucleotide pyrophosphatase/phosphodiesterase 2 (autotaxin)	T80232	Hs.190977
21453	1	0.26	4.30E-07	Ectonucleotide pyrophosphatase/phosphodiesterase 2 (autotaxin)	AA476508	Hs.190977
21223	0.88	0.28	3.50E-03		AA775616	Data not found
20672	0.85	1.5	1.10E-02	v-kit hardy-zuckerman 4 feline sarcoma viral oncogene homolog	N24824	Hs.479754
10064	0.78	2	2.20E-02	v-rel reticuloendotheliosis viral oncogene homolog b, nuclear factor of kappa light polypeptide gene enhancer in b-cells 3 (avian)	AA258001	Hs.307905
18012	0.78	2.2	2.10E-04		T63324	Data not found
21141	0.78	2.4	6.40E-03	Apolipoprotein d	AA456975	Hs.522555
13460	0.77	2	3.50E-04	Major histocompatibility complex, class ii, dr beta 4	AA630549	Hs.534322
20835	0.77	2.2	1.20E-03	Major histocompatibility complex, class i, a	AA644657	Hs.181244
22167	0.7	3.6	2.40E-03	Serum/glucocorticoid regulated kinase	AA486082	Hs.296323
20383	0.63	2	4.70E-04	Major histocompatibility complex, class ii, dp beta 1	AA486627	Hs.485130
20697	0.62	2	1.50E-03	Major histocompatibility complex, class ii, dr beta 4	W88967	Hs.534322
13282	0.6	2.1	2.20E-03	Phospholipase a2, group iia (platelets, synovial fluid)	T61323	Hs.466804
20266	0.58	1.9	2.40E-03	Chemokine (c-c motif) ligand 14	R96668	Hs.272493
20834	0.58	2.1	9.80E-04	Major histocompatibility complex, class ii, dr beta 4	AA664195	Hs.520049
20980	0.58	2.1	1.50E-04	Major histocompatibility complex, class ii, dp alpha 1	AA634028	Hs.347270
20258	0.55	1.8	5.10E-03	Major histocompatibility complex, class ii, dr alpha	R47979	Hs.520048
21313	0.55	2	2.40E-03	Major histocompatibility complex, class ii, dr beta 6 (pseudogene)	H50623	Hs.545653
20804	0.5	1.5	1.70E-02		H26426	Data not found
13089	0.43	2	6.00E-04	Growth differentiation factor 10	R52085	Hs.2171
20828	0.43	0.51	1.20E-02	Microfibrillar-associated protein 2	N67487	Hs.389137
10161	0.42	1.8	2.00E-02	abl interactor 2	N21334	Hs.471156
21955	0.42	1.9	4.70E-04	Microsomal glutathione s-transferase 2	W73474	Hs.81874
13525	0.38	1.8	9.40E-03	Procollagen-proline, 2-oxoglutarate 4-dioxygenase (proline 4-hydroxylase), alpha polypeptide i	AA457671	Hs.500047
21888	0.33	2.6	3.60E-04	Inositol 1,4,5-triphosphate receptor, type 2	R68021	Hs.512235
18020	0.32	1.8	8.90E-03	Major histocompatibility complex, class i, a	AA644657	Hs.181244
22181	0.32	1.4	1.60E-02	grb2-associated binding protein 1	R96595	Hs.80720
21553	0.3	1.4	2.40E-02	Tumour necrosis factor, alpha-induced protein 2	W33183	Hs.525607
22288	0.3	1.5	1.20E-02	Matrix metalloproteinase 7 (matrilysin, uterine)	AA031513	Hs.2256
22318	0.28	1.6	1.50E-02	Cadherin 1, type 1, e-cadherin (epithelial)	H97778	Hs.461086
18030	0.27	2	6.20E-03	Homo sapiens, clone image: 5575764, mRNA	W60701	Hs.519978
20784	0.27	0.51	1.20E-02	Tissue inhibitor of metalloproteinase 3 (sorsby fundus dystrophy, pseudoinflammatory)	AA099153	Hs.297324
21105	0.27	0.42	1.30E-05	Similar to ribosomal protein l18a; 60s ribosomal protein l18a	W81118	Hs.517776
22532	0.25	0.51	9.40E-03	Tissue inhibitor of metalloproteinase 3 (sorsby fundus dystrophy, pseudoinflammatory)	AA479202	Hs.297324
13243	0.23	0.52	1.50E-02	Tissue inhibitor of metalloproteinase 3 (sorsby fundus dystrophy, pseudoinflammatory)	AA479202	Hs.297324
20723	0.23	1.4	1.70E-02		AA455270	Data not found
21887	0.23	1.3	2.10E-02	rab2, member ras oncogene family	T82415	Hs.369017
22206	0.23	2.6	1.20E-03	Macrophage stimulating, pseudogene 9	T51539	Hs.475654
22253	0.23	1.4	2.90E-03	rab2, member ras oncogene family	R38260	Hs.369017
20934	0.22	1.4	2.70E-02	Nuclear factor of activated t-cells, cytoplasmic, calcineurin-dependent 1	AA679278	Hs.534074
21025	0.22	0.44	5.40E-05	Zinc finger protein 9 (a cellular retroviral nucleic acid binding protein)	AA625995	Hs.518249
21119	0.22	2.2	4.00E-03	Homo sapiens, clone image: 5575764, mRNA	W60701	Hs.519978
21372	0.22	1.9	3.50E-04	cug triplet repeat, RNA binding protein 2	T84491	Hs.309288

*Gene number used in the array data.
†The average selection rate.
‡The ratio between the means of the two molecular classes.
§p Value from the Wilcoxon rank sum test on the two molecular classes.
All other columns are from the original data provided. Genes 20194 and 21453, which correspond to one unique gene alone, can classify the molecular classes detected using all the data.

a 30 µl reaction mixture containing annealed RNA template, first-strand buffer, 500 µM (each) dATP, dCTP, and dGTP, 300 µM dTTP, 200 µM aminoallyl-dUTP (Sigma), 10 mM dithiothreitol, and 12.7 units of Superscript II per µl. For template hydrolysis, 10 µl of 0.1 M NaOH was added to the reverse transcription reaction mixture and the mixture was incubated for 10 min at 70℃, allowed to cool at room temperature for 5 min, and neutralised by the addition of 10 µl of 0.1 M HCl. cDNA was precipitated at −20℃ for 30 min after the addition of 1 µl of linear acrylamide (Ambion), 4 µl of 3 M sodium acetate (pH 5.2), and 100 µl of absolute ethanol, and then resuspended in 5 µl of 0.1 M NaHCO3. For dye coupling, the contents of one tube of *N*-hydroxysuccinimide ester containing Cy3 or Cy5 dye (product numbers PA25001 and PA25002; GE Healthcare) was dissolved in 45 µl of dimethyl sulfoxide. Five µl of dye solution was mixed with the cDNA and incubated for 1 h in darkness at room temperature. Labelled cDNA was purified on a QIAquick PCR purification column (QIAGEN) according to the manufacturer's instructions. Eluted cDNA was dried under a vacuum and resuspended in 30 µl of Slidehyb II hybridisation buffer (Ambion). After 2 min of denaturation at 95℃, the hybridisation mixture was applied to the microarray slide under a coverslip. Hybridisation proceeded overnight in a sealed moist chamber in a 55℃ water bath. After hybridisation, slides were washed successively for 5 min each in 2× SSC–0.1% SDS at 55℃, then in 2× SSC at 55℃, and finally in 0.2× SSC at room temperature.

Acquisition of data

Data were acquired with a GenePix 4000B laser scanner and GenePix Pro software, version 5.0, as previously described.[22]

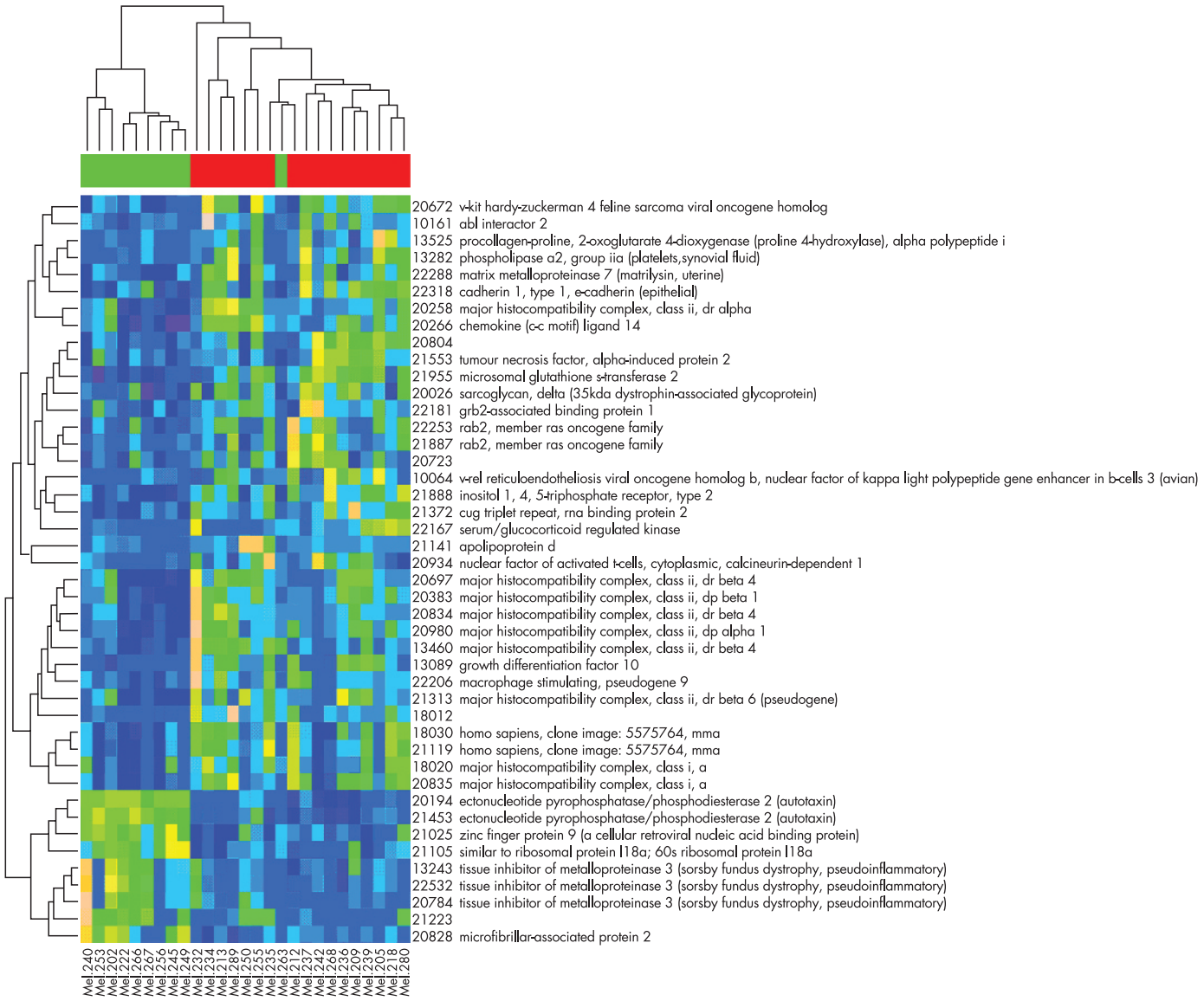

Figure 5 Gene profiles of the 44 key genes across the 27 samples with the dendrogram from the samples on the top and the dendrogram from the 44 key genes on the side. Pink indicates the high expression and cerulean blue indicates low expression. The colour bar on the top indicates the metastatic death status—green for alive and red for dead. The 44 key genes are clustered into two major groups shown in the site dendrogram: one group has high expressions in molecular class 1 and low expressions in molecular class 2 and the other low in molecular class 1 and high in molecular class 2.

Real-time quantitative PCR

One µg of total RNA was reverse transcribed using random hexamers (Superscript first-strand synthesis system; Invitrogen). Real-time quantitative RTQ-PCR was performed on the cDNA using a Taqman gene expression assay for autotaxin (Hs00196470 µm1) normalised with a eukaryotic 18S rRNA endogenous control assay (Applied Biosystems, Foster City, CA, USA). Reactions were performed in triplicate on a 7900HT Sequence Detection System instrument (Applied Biosystems) using Real Master Mix Probe ROX according to the manufacturers instructions (Eppendorf). Relative quantification was determined by comparison of each sample to a reference cDNA (Universal human reference RNA, Stratagene, La Jolla, CA).

Data analysis

Two multivariate data mining techniques, Hierarchical cluster analysis performed with 10 000 randomly selected subsets and multidimensional scaling,[26] were used to investigate the grouping structure in the gene expression data of the 27 tumour samples. Pearson correlation coefficient was used as the proximity matrix[27] in the hierarchical cluster analysis and in multidimensional scaling. Hierarchical cluster analysis with average linkage method[26] was used to generate the dendrograms. Multidimensional scaling was also applied to investigate the grouping structure. Tumour metastatic survival data within molecular classes was correlated with Kaplan–Meier survival curves.

RESULTS

Clinical aspects

Twenty seven patients were included in the study. The average age of the patients was 61 years, of whom 13 were female; 16 patients were dead by the follow-up date. The clinical details, tumour features, histopathological features and outcome are summarised in table 1.

Gene expression profile analysis

No obvious pitfalls were found when we looked at the overall gene expression profiles across the tumour samples, so we

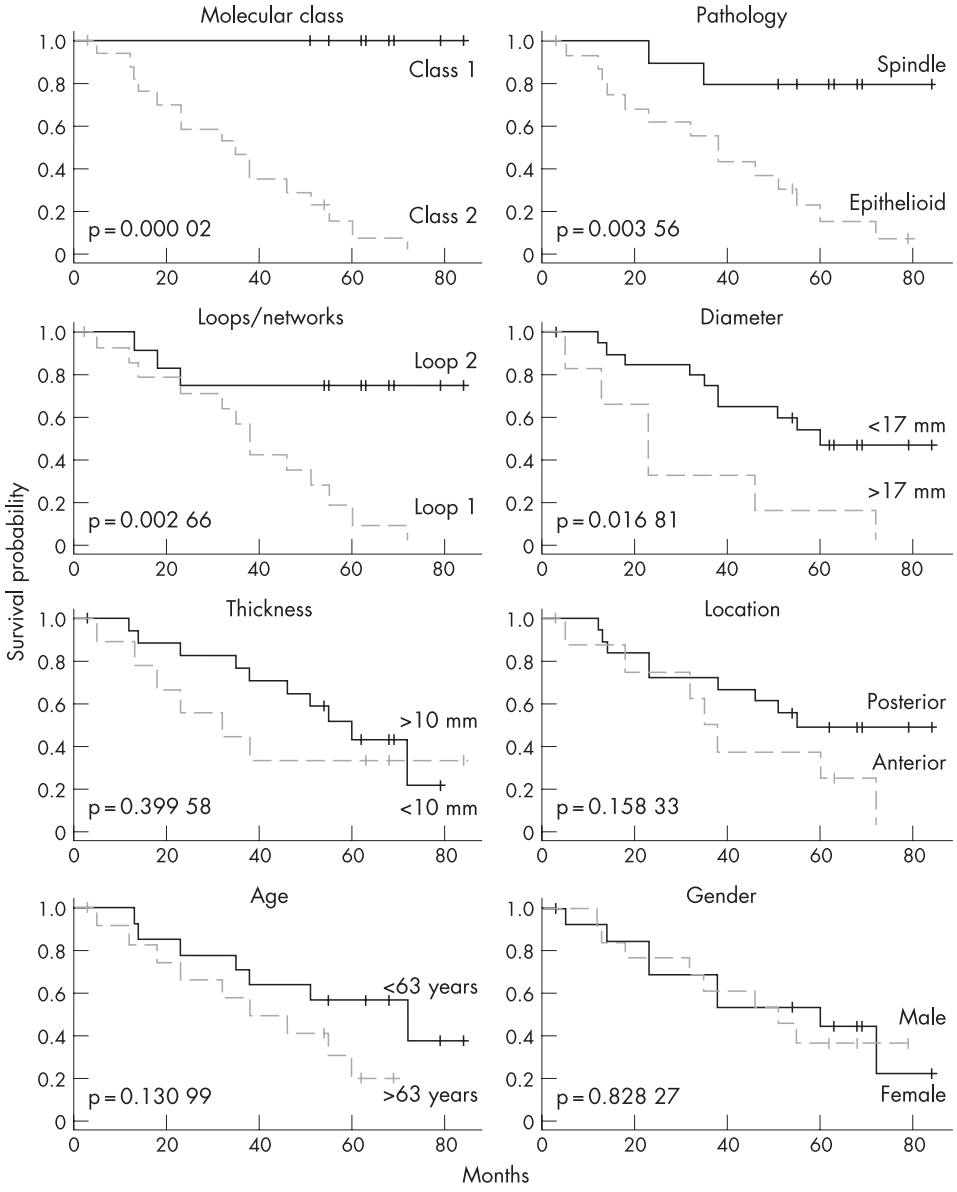

Figure 6 Kaplan–Meier survival analysis on molecular classes and seven histopathological and clinical measures. All mortality was melanoma metastasis. Statistical significance is based on log-rank test and indicated in the plot for each parameter.

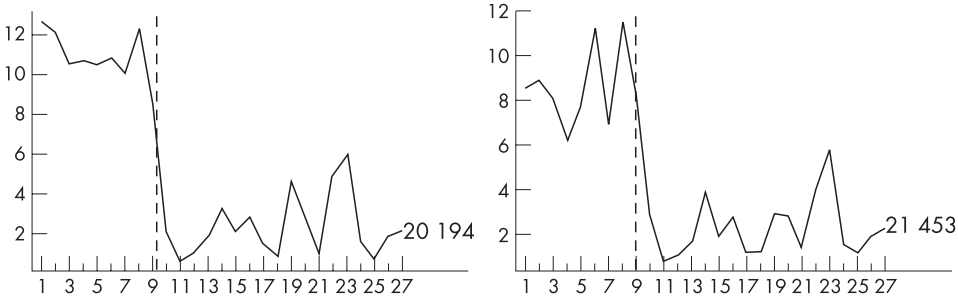

Figure 7 Individual profile for ENPP2 expression (autotaxin, 20194). The x axis corresponds to 27 samples that are grouped onto molecular class 1 and class 2, in that order, and the dashed vertical lines indicates the boundary between the two classes. Note lower expression in molecular class 2 sample.

analysed all 27 samples provided (fig 1). Hierarchical cluster analysis revealed two distinct molecular classes (class 1 and class 2). Hierarchical cluster analysis with average linkage method was used to generate the dendrogram (fig 2). Multidimensional scaling analysis also revealed two molecular classes identical to those found with the hierarchical cluster analysis (fig 3).

Key genes that are in favour of the grouping structure

We next identified the genes that distinguished the two molecular classes. First, all genes were pre-filtered and those with data missing were deleted. Wilcoxon rank sum test was performed on the remaining 3514 genes. Based on the p values from the Wilcoxon test, the adjusted p values for controlling the false discovery rate were calculated. We filtered out all the

Table 3 Comparison of top discriminating genes from published studies that are underexpressed in class 2 (poor prognosis) uveal melanoma

Present study	Tschentscher[17]	Onken[19]	Worley[39]
ENPP2	CHL1	**ENPP2**	**LPIN1**
MAP2	HIFX	**PHLDA1**	**ENPP2**
TIMP3	CLONE 24421	**FZD6**	LMCD1
RIB118a	PDE3A		SLC6A15
ZFP9	*fls485*		
	ROBO1		
	HCGIV.9		
	IL12RB2		
	SPP1		
	PDE4B		
	MSC		
	TIMP3		
	ATIP1		
	KIAA0828		
	PHLDA1		
	PLXNB1		
	COX8A2		
	KIAA0977		
	8ETMAR		
	PTRF		
	FZD6		
	PPP13RC		
	ET81		
	IL1RAP		
	ID2		
	NR1D2		
	36b3cDNA		
	ALDH5A1		
	RAF1		
	TFAP2A		
	NTT73		
	ADFP		
	LPIN1		

Genes found to be discriminating in more than one study are shown in bold.

genes with false discovery rate adjusted p values greater than 0.1, leaving 972 genes. Second, cluster analysis was repeatedly performed with 10 000 randomly selected subset of genes, and the cumulative contributions of all the genes in making the correct grouping were recorded. The cumulative contribution (score) was plotted for all 972 genes and we selected the top 32 discrete genes (corresponding to 44 probe sets) with the highest classification contribution (fig 4; indicated as red dots). The 44 probe sets selected from the above algorithm are listed in table 2. The 44 probe sets are clustered into two major groups, with either high expression of molecular class 1 and low expression of molecular class 2, or low expression of class 1 and high expression of class 2 (fig 5).

Correlation with survival data

The two molecular classes corresponded very well to the Kaplan–Meier survival curves of the two classes. Class 1 had all nine patients alive and class 2 had 17 dead and one alive patient. The prognosis obtained with molecular classification was superior to other well known prognosticators such as tumour size, histopathology, location and extracellular matrix patterns (fig 6).[28] Moreover, among the 32 key genes, gene expression pattern of autotaxin (ectonucleotide pyrophosphatase-phosphodiesterase 2, ENPP2) alone was sufficient to distinguish molecular class 1 and class 2, where class 2 represents poor prognosis uveal melanoma (fig 7). The expression pattern of autotaxin was confirmed using real-time quantitative PCR (in triplicate) and was highly concordant.

DISCUSSION

Uveal melanoma cells are shed into circulation at initial presentation and even in adequately treated cases.[29] The fate of the uveal melanoma cells in the circulation and hence the features that influence their ability to establish metastasis determines the survival of patients with uveal melanoma. Microarray gene profiling is a powerful tool that can reveal such genetic attributes. In our study, cluster analysis performed with a subset of 10 000 randomly selected genes revealed 44 genes with the highest classification contribution and cumulative contribution (score). Overexpression of E-cadherin was noted in class 2 uveal melanoma associated with poor prognosis. E-cadherin is an important transmembrane protein which is indicative of epithelial differentiation.[30] This attribute correlates with epithelial cell-like (epithelioid) morphology of aggressive uveal melanoma.[31] Although overexpression of E-cadherin in class 2 uveal melanoma associated with poor prognosis initially appears to be paradoxical, E-cadherin is also upregulated in other cancers that spread haematogenously, such as advanced cutaneous melanoma and hepatocellular carcinoma.[32]

In the circulation, uveal melanoma cells with high HLA class I expression enable the cells to evade natural killer cell-mediated tumour surveillance.[33] Therefore, it is not unexpected that several genes of the histocompatibility complex class I and class II were overexpressed in class 2 uveal melanoma associated with a poor prognosis. It is also likely that the presence of tumour-infiltrating macrophages and lymphocytes, features of a poor prognosis for uveal melanoma,[34] may be the reason for the observed overexpression of immune response genes.

Tissue inhibitor of metalloproteinase 3 (TIMP3) inhibits cell invasion and metastasis by inhibiting degradation of the extracellular matrix.[35] TIMP3 also induces apoptosis[36] and inhibits angiogenesis.[37] Comparative expression profiling of metastasis in uveal melanoma cell lines and primary uveal melanoma cell lines revealed a fivefold lower expression of TIMP3 in metastasis cell lines.[38] The lower expression of TIMP3 in class 2 uveal melanoma with a poor prognosis, as observed in our study, indicates pro-angiogenic and anti-apoptotic attributes of aggressive melanoma cells that favour establishment of tumour metastatic sites.

Results of gene expression profiling do not always generate reproducible or identical genetic profiles due to several factors including biological and technical variability (table 3). Previous studies have identified sets of 201 genes,[17] 7 genes,[39] and 3 genes[19] sufficient for accurate class prediction in uveal melanoma. It is remarkable that autotaxin was also one of the discriminating genes in two previous studies.[19 39] In any event, it is prudent not to focus on one gene; the expression pattern of several genes should be considered for determining the expression profile.[40] What is remarkable is the fact that non-metastasising (class 1) and metastasising (class 2) uveal melanoma can be readily discriminated by their genetic profiles as determined by microarray techniques.

Autotaxin is synthesised as a pre-pro-enzyme and after proteolytic cleavage the protein is secreted.[41] Autotaxin is identical to lysophospolipase D and generates lysophosphatidic acid by hydrolysing lysophosphatidyl choline.[42] Lysophosphatidyl choline enhances cell motility, cell proliferation, and angiogenesis[41 43 44] through G protein-coupled receptors.[45] Autotaxin is upregulated in various malignancies, including breast,[46] lung,[47] thyroid carcinoma[48] and glioblastoma multiforme.[49]

As autotaxin is a tumour cell motility-stimulating factor, originally isolated from melanoma cell supernatants,[50] it is possible that autotaxin may be detected in serum and serve as a biomarker of metastasis. Underexpression of autotaxin in class 2 uveal melanoma with a poor prognosis needs to be explored further.

Authors' affiliations

A D Singh, Cole Eye Institute, Cleveland Clinic Foundation, Cleveland, OH, USA
K Sisley, H S Mudhar, I G Rennie, Ophthalmology and Histopathology, Royal Hallamshire Hospital, Sheffield, UK
Y Xu, J Li, Quantitative Health Sciences, Cleveland Clinic Foundation, Cleveland, OH, USA
P Faber, S J Plummer, P M Kessler, G Casey, Cancer Biology, Cleveland Clinic Foundation, Cleveland, OH, USA
B G Williams, Monash Institute of Medical Research, Monash University, Melbourne, Australia

Grant support: American Cancer Society.

Competing interests: None declared.

REFERENCES

1 **Singh AD**, Topham A. Incidence of uveal melanoma in the United States: 1973–1997. *Ophthalmology* 2003;**110**:956–61.
2 **Singh AD**, Bergman L, Seregard S. Uveal malignant melanoma: epidemiologic aspects. In: Singh AD, Damato BE, Pe'er J, *et al*, eds. *Clinical ophthalmic oncology*. Philadelphia: Saunders-Elsevier, 2007:198–204.
3 **Egan KM**, Seddon JM, Glynn RJ, *et al*. Epidemiologic aspects of uveal melanoma. *Surv Ophthalmol* 1988;**32**:239–51.
4 **Singh AD**, Bergman L, Seregard S. Uveal melanoma: epidemiologic aspects. *Ophthalmol Clin North Am*. 2005;18: 75–84, viii).
5 **Diener-West M**, Hawkins BS, Markowitz JA, *et al*. A review of mortality from choroidal melanoma. *Arch Ophthalmol* 1992;**110**:245–50.
6 **Anonymous**. The COMS randomized trial of iodine 125 brachytherapy for choroidal melanoma, III: initial mortality findings. COMS report no. 18. *Arch Ophthalmol* 2001;**119**:969–82.
7 **Anonymous**. The Collaborative Ocular Melanoma Study (COMS) randomized trial of pre-enucleation radiation of large choroidal melanoma II: initial mortality findings. COMS report no. 10. *Am J Ophthalmol* 1998;**125**:779–96.
8 **Anonymous**. Mortality in patients with small choroidal melanoma. COMS report no. 4. The Collaborative Ocular Melanoma Study Group. *Arch Ophthalmol* 1997;**115**:886–93.
9 **Kujala E**, Makitie T, Kivela T. Very long-term prognosis of patients with malignant uveal melanoma. *Investigative Ophthalmology & Visual Science* 2003;**44**:4651–9.
10 **Singh AD**, Borden EC. Metastatic uveal melanoma. *Ophthalmol Clin North Am*. 2005;18: 143–50, ix).
11 **Anonymous**. Accuracy of diagnosis of choroidal melanomas in the Collaborative Ocular Melanoma Study. COMS report no. 1. *Arch Ophthalmol* 1990;**108**:1268–73.
12 **Singh AD**, Topham A. Survival rates with uveal melanoma in the United States: 1973–1997. *Ophthalmology* 2003;**110**:962–5.
13 **Prescher G**, Bornfeld N, Becher R. Nonrandom chromosomal abnormalities in primary uveal melanoma. *J Natl Cancer Inst* 1990;**82**:1765–9.
14 **Prescher G**, Bornfeld N, Hirche H, *et al*. Prognostic implications of monosomy 3 in uveal melanoma. *Lancet* 1996;**347**:1222–5.
15 **Singh AD**, Boghosian-Sell L, Wary KK, *et al*. Cytogenetic findings in primary uveal melanoma. *Cancer Genetics & Cytogenetics* 1994;**72**:109–15.
16 **Sisley K**, Rennie IG, Parsons MA, *et al*. Abnormalities of chromosomes 3 and 8 in posterior uveal melanoma correlate with prognosis. *Genes, Chromosomes & Cancer* 1997;**19**:22–8.
17 **Tschentscher F**, Husing J, Holter T, *et al*. Tumor classification based on gene expression profiling shows that uveal melanomas with and without monosomy 3 represent two distinct entities. *Cancer Res* 2003;**63**:2578–84.
18 **Zuidervaart W**, van der Velden PA, Hurks MH, *et al*. Gene expression profiling identifies tumour markers potentially playing a role in uveal melanoma development. *Br J Cancer* 2003;**89**:1914–19.
19 **Onken MD**, Worley LA, Ehlers JP, *et al*. Novel molecular classification of uveal melanoma reveals two molecular classes and predicts metastatic death. *Cancer Res* 2004;**64**:7205–9.
20 **Folberg R**, Pe'er J, Gruman LM, *et al*. The morphologic characteristics of tumor blood vessels as a marker of tumor progression in primary human uveal melanoma: a matched case-control study. *Hum Pathol* 1992;**23**:1298–305.
21 **Folberg R**, Rummelt V, Parys-Van Ginderdeuren R, *et al*. The prognostic value of tumor blood vessel morphology in primary uveal melanoma. *Ophthalmology* 1993;**100**:1389–98.
22 **Wang E**, Miller LD, Ohnmacht GA, *et al*. High-fidelity mRNA amplification for gene profiling. *Nat Biotechnol* 2000;**18**:457–9.
23 **Li W**, Kessler P, Williams BR. Transcript profiling of Wilms tumors reveals connections to kidney morphogenesis and expression patterns associated with anaplasia. *Oncogene* 2005;**24**:457–68.
24 **Li W**, Kessler P, Yeger H, *et al*. A gene expression signature for relapse of primary wilms tumors. *Cancer Res* 2005;**65**:2592–601.
25 **Frevel MA**, Bakheet T, Silva AM, *et al*. p38 Mitogen-activated protein kinase-dependent and -independent signaling of mRNA stability of AU-rich element-containing transcripts. *Mol Cell Biol* 2003;**23**:425–36.
26 **Hastie T**, Tibshirani R, Friedman J. *The elements of statistical learning*. New York: Springer Verlag, 2001.
27 **Eisen MB**, Spellman PT, Brown PO, *et al*. Cluster analysis and display of genome-wide expression patterns. *Proc Natl Acad Sci U S A* 1998;**95**:14863–8.
28 **Singh AD**, Shields CL, Shields JA. Prognostic factors in uveal melanoma. *Melanoma Research* 2001;**11**:1–9.
29 **Callejo SA**, Antecka E, Blanco PL, *et al*. Identification of circulating malignant cells and its correlation with prognostic factors and treatment in uveal melanoma. A prospective longitudinal study. *Eye* 2006.
30 **Haass NK**, Smalley KS, Li L, *et al*. Adhesion, migration and communication in melanocytes and melanoma. *Pigment Cell Res* 2005;**18**:150–9.
31 **Hendrix MJ**, Seftor EA, Seftor RE, *et al*. Biologic determinants of uveal melanoma metastatic phenotype: role of intermediate filaments as predictive markers. *Lab Invest* 1998;**78**:153–63.
32 **Onken MD**, Ehlers JP, Worley LA, *et al*. Functional gene expression analysis uncovers phenotypic switch in aggressive uveal melanomas. *Cancer Res* 2006;**66**:4602–9.
33 **Jager MJ**, Hurks HM, Levitskaya J, *et al*. HLA expression in uveal melanoma: there is no rule without some exception. *Hum Immunol* 2002;**63**:444–51.
34 **Makitie T**, Summanen P, Tarkkanen A, *et al*. Tumor-infiltrating macrophages (CD68(+) cells) and prognosis in malignant uveal melanoma. *Invest Ophthalmol Vis Sci* 2001;**42**:1414–21.
35 **Hojilla CV**, Mohammed FF, Khokha R. Matrix metalloproteinases and their tissue inhibitors direct cell fate during cancer development. *Br J Cancer* 2003;**89**:1817–21.
36 **Ahonen M**, Baker AH, Kahari VM. Adenovirus-mediated gene delivery of tissue inhibitor of metalloproteinases-3 inhibits invasion and induces apoptosis in melanoma cells. *Cancer Res* 1998;**58**:2310–15.
37 **Handsley MM**, Edwards DR. Metalloproteinases and their inhibitors in tumor angiogenesis. *Int J Cancer* 2005;**115**:849–60.
38 **van der Velden PA**, Zuidervaart W, Hurks MH, *et al*. Expression profiling reveals that methylation of TIMP3 is involved in uveal melanoma development. *Int J Cancer* 2003;**106**:472–9.
39 **Worley LA**, Onken MD, Person E, *et al*. Transcriptomic versus chromosomal prognostic markers and clinical outcome in uveal melanoma. *Clin Cancer Res* 2007;**13**:1466–71.
40 **Conlon MR**, Albert DM. Uveal melanoma. *International Ophthalmology Clinics* 1993;**33**:67–76.
41 **Jansen S**, Stefan C, Creemers JW, *et al*. Proteolytic maturation and activation of autotaxin (NPP2), a secreted metastasis-enhancing lysophospholipase D. *J Cell Sci* 2005;**118**:3081–9.
42 **Umezu-Goto M**, Kishi Y, Taira A, *et al*. Autotaxin has lysophospholipase D activity leading to tumor cell growth and motility by lysophosphatidic acid production. *J Cell Biol* 2002;**158**:227–33.
43 **Nam SW**, Clair T, Kim YS, *et al*. Autotaxin (NPP-2), a metastasis-enhancing motogen, is an angiogenic factor. *Cancer Res* 2001;**61**:6938–44.
44 **Umezu-Goto M**, Tanyi J, Lahad J, *et al*. Lysophosphatidic acid production and action: validated targets in cancer? *J Cell Biochem* 2004;**92**:1115–40.
45 **Moolenaar WH**, van Meeteren LA, Giepmans BN. The ins and outs of lysophosphatidic acid signaling. *Bioessays* 2004;**26**:870–81.
46 **Yang SY**, Lee J, Park CG, *et al*. Expression of autotaxin (NPP-2) is closely linked to invasiveness of breast cancer cells. *Clin Exp Metastasis* 2002;**19**:603–8.
47 **Yang Y**, Mou L, Liu N, *et al*. Autotaxin expression in non-small-cell lung cancer. *Am J Respir Cell Mol Biol* 1999;**21**:216–22.
48 **Kehlen A**, Englert N, Seifert A, *et al*. Expression, regulation and function of autotaxin in thyroid carcinomas. *Int J Cancer* 2004;**109**:833–8.
49 **Kishi Y**, Okudaira S, Tanaka M, *et al*. Autotaxin is overexpressed in glioblastoma multiforme and contributes to cell motility of glioblastoma by converting lysophosphatidylcholine to lysophosphatidic acid. *J Biol Chem* 2006;**281**:17492–500.
50 **Stracke ML**, Krutzsch HC, Unsworth EJ, *et al*. Identification, purification, and partial sequence analysis of autotaxin, a novel motility-stimulating protein. *J Biol Chem* 1992;**267**:2524–9.